AIAA 98-0519
Spatial Characteristics of the Unsteady Differential Pressures on 16% F/A-18 Vertical Tails

Robert W. Moses, Ph.D.
NASA Langley Research Center
Hampton, VA

Holt Ashley, Professor Emeritus
Department of Aeronautics & Astronautics
Stanford University
Stanford, CA

36th Aerospace Sciences Meeting & Exhibit
January 12–15, 1998 / Reno, NV

AIAA-98-0519

SPATIAL CHARACTERISTICS OF THE UNSTEADY DIFFERENTIAL PRESSURES ON 16% F/A-18 VERTICAL TAILS

Robert W. Moses, Ph.D.
AIAA Member
Aeroelasticity Branch
NASA Langley Research Center
Hampton, VA

Holt Ashley, Professor Emeritus
AIAA Honorary Fellow
Department of Aeronautics & Astronautics
Stanford University
Stanford, CA

Abstract

Buffeting is an aeroelastic phenomenon which plagues high performance aircraft at high angles of attack. For the F/A-18 at high angles of attack, vortices emanating from wing/fuselage leading edge extensions burst, immersing the vertical tails in their turbulent wake. The resulting buffeting of the vertical tails is a concern from fatigue and inspection points of view.

Previous flight and wind-tunnel investigations to determine the buffet loads on the tail did not provide a complete description of the spatial characteristics of the unsteady differential pressures. Consequently, the unsteady differential pressures were considered to be fully correlated in the analyses of buffet and buffeting. The use of fully correlated pressures in estimating the generalized aerodynamic forces for the analysis of buffeting yielded responses that exceeded those measured in flight and in the wind tunnel.

To learn more about the spatial characteristics of the unsteady differential pressures, an available 16%, sting-mounted, F-18 wind-tunnel model was modified and tested in the Transonic Dynamics Tunnel (TDT) at the NASA Langley Research Center as part of the ACROBAT (Actively Controlled Response Of Buffet-Affected Tails) program. Surface pressures were measured at high angles of attack on flexible and rigid tails. Cross-correlation and cross-spectral analyses of the pressure time histories indicate that the unsteady differential pressures are not fully correlated. In fact, the unsteady differential pressures resemble a wave that travels along the tail. At constant angle of attack, the pressure correlation varies with flight speed.

Introduction

Buffeting is an aeroelastic phenomenon which plagues high performance aircraft, especially those with twin vertical tails. For aircraft of this type at high angles of attack, vortices emanating from wing/fuselage leading edge extensions burst, immersing the vertical tails in their wake, as shown in Figure 1. The resulting buffeting of the vertical tails is a concern from fatigue and inspection points of view. Previous wind-tunnel and flight tests were conducted to quantify the buffet loads on the vertical tails.

The spectral aspects of the unsteady differential pressures on the vertical tail caused by a burst LEX (leading edge extension) vortex are well documented.[1] The results of Reference 1 illustrate the variations of the power spectral densities and root mean square (rms) values of the differential pressures with flight speed, angle of attack (AOA),

dynamic pressure, and tail coordinate using only five differential pressure transducers.[1] In Reference 1, the worst case condition, defined by the highest rms values of differential pressure at design limit load, occurs around 340 psf and 32 degrees angle of attack. Other findings were that the root mean square value of the differential pressure varies linearly with dynamic pressure, and that Strouhal scaling provides a means for comparing model and flight data. Also, the highest rms values occurred at stations closest to the leading edge while the lowest rms values occurred near the trailing edge with a gradual change in rms values between these two regions of the tail. The reasons for this gradual reduction in the rms values with increase in chord coordinate were not explained. During the investigation, the unsteady differential pressures were considered fully correlated (in phase) because their results of the pressures measured at only five stations did not indicate otherwise. The sampling rate used in this test is not clearly reported.

Figure 1. Flow Visualization of Leading Edge Extension (LEX) Vortex Burst, 30 Degrees Angle of Attack

After the research of Reference 1 and prior to the research reported herein, wind-tunnel tests were conducted to investigate the spatial characteristics of the unsteady surface pressures on the tail.[2] Contour plots of the time delays on each surface were constructed using cross-correlation analyses of the unsteady pressures measured on each tail surface of a 6% rigid F/A-18 model tested at Mach 0.6. As shown in Figure 2 for 35 degrees angle of attack, the contours for each surface are quite different. The spatial characteristics of the unsteady differential pressures are unclear from examination of these plots of the unsteady pressures on each surface. On the inboard surface at 35 degrees angle of attack and Mach 0.6, the time delay from a station near the leading edge to a station near the trailing edge is approximately 0.0006 seconds. The sampling rate is not clearly reported; however, a time delay of 0.0006 seconds indicates that a high sampling rate is needed to capture the convection of the flow.

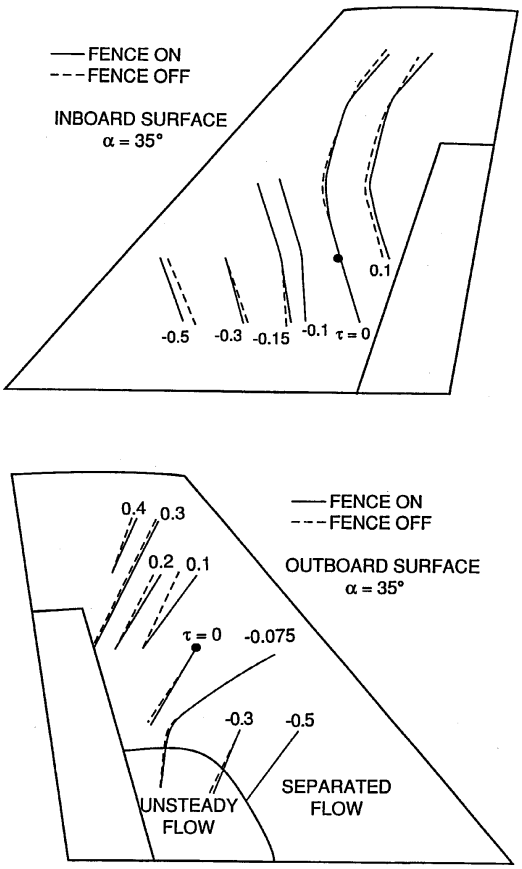

Figure 2. Peak Correlation Contours (msec) of the Fin Unsteady Pressure Signals, 6% Rigid Tail, M=0.6, 35 Degrees AOA (From Reference 2)

Because little information was known regarding their spatial correlation, the differential pressures on the tail were assumed to be zero- or fully-correlated during the computations of the generalized aerodynamic forces.[3-5] These analyses did not estimate the buffeting accurately. After further study, it was concluded that the issue of pressure correlation is the key to successful buffeting prediction and should be the subject of more research.[4-5]

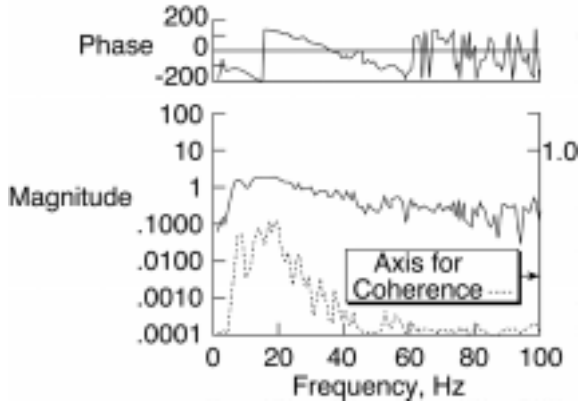

a) 20 Degrees AOA

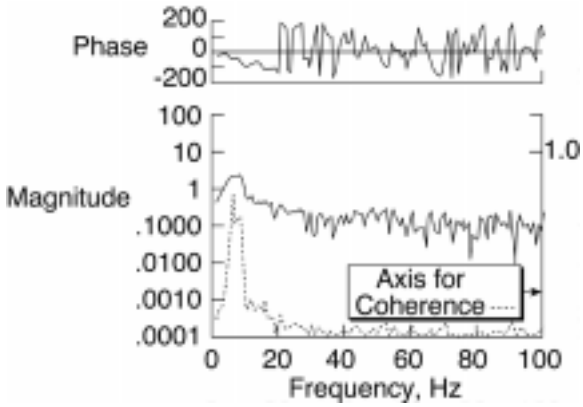

b) 32 Degrees AOA

Figure 3. Cross-Spectral Density and Coherence Functions Between the Differential Pressures Near the Leading-Edge Tip and the Trailing-Edge Tip, Full-Scale Tail, M=0.15, (From Reference 6)

To learn more about the pressure correlation, a full-scale F/A-18 was tested at high angles of attack at a maximum speed of Mach 0.15 in a wind tunnel. Plots of the magnitudes and phase delays of the unsteady differential pressures were constructed using cross-spectral analyses of the unsteady pressures measured on each tail surface at Mach 0.15.[6-7] As shown in Figure 3a for 20 degrees AOA, the phase is approximately negative 400 degrees (-360-40) at 45 Hz, which is the frequency of the first torsion mode of the tail. As shown in Figure 3b for 32 degrees angle of attack, the phase is approximately negative -180 degrees at 20 Hz. In Figure 3b, the phase values at frequencies above 20 Hz are difficult to determine because of the wrapping used in plotting the phase. Although flight conditions were not matched, the results of this wind-tunnel test indicate that the differential pressures acting on the tail are not in phase. However, the dependencies of pressure correlation on flight conditions were not clearly understood from these results.

To better understand the pressure correlation during buffet, an available 16%, sting-mounted, F-18 wind-tunnel model was modified and tested in the Transonic Dynamics Tunnel (TDT) at the NASA Langley Research Center as part of the ACROBAT (Actively Controlled Response Of Buffet-Affected Tails) program.[8] Surface pressures were measured for scaled flight conditions at high angles of attack on flexible and rigid tails. Pressure signals were sampled at 6538 Hz for approximately 30 seconds. Cross-correlation and time-averaged cross-spectral analyses [9] were performed for identifying any consistent spatial characteristics of the unsteady differential pressures. The results of these analyses indicate that the unsteady differential pressures are not fully correlated. In fact, the unsteady differential pressures resemble a wave that travels along the tail.

The purpose of this paper is to present some wind-tunnel results that illustrate the partial correlation of the unsteady differential buffet pressures on a rigid tail and a flexible tail of a 16% F/A-18 model.

Wind-Tunnel Model and Tunnel Conditions

An existing 16% (also referred to as 1/6-scale), rigid, full-span model of the F/A-18 A/B aircraft was refurbished, and three flexible and two rigid vertical tails were fabricated. This model was then sting-mounted in the Transonic Dynamics Tunnel (TDT) at the NASA Langley Research Center, as shown in Figure 4, where it underwent a series of tests to determine buffet flowfield characteristics and to alleviate vertical tail buffeting using active controls.[8]

The three flexible tails were fabricated from a 1/8-inch thick aluminum plate and covered with balsa wood. The aluminum plate thickness was chosen such that the frequencies and shapes of the first three modes were close to those of the actual tail as determined by a finite element analysis. All three flexible tails were instrumented with a root strain gage aligned to measure bending moment and with two tip accelerometers near the leading and trailing edges. The two rigid tails (one port,

one starboard) were fabricated from a block of aluminum and were geometrically identical to the flexible tails. Two of the flexible tails and both rigid tails were instrumented with unsteady pressure transducers for measuring pressures on both surfaces of the tails, as shown in Figures 5 and 6, respectively. At each station, there are two transducers, one on each side of the tail.

Figure 4. 1/6-Scale F/A-18 Model Mounted in the Transonic Dynamics Tunnel

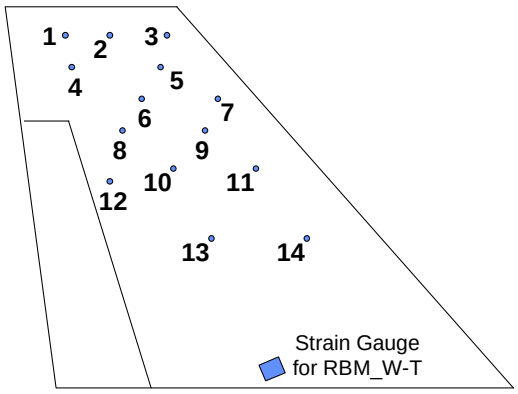

Figure 5. Pressure Transducer Stations, 1/6-Scale Flexible Tail

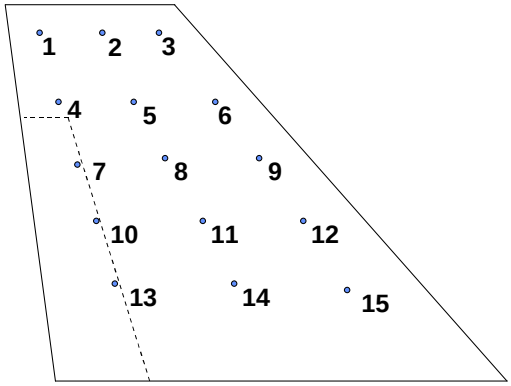

Figure 6. Pressure Transducer Stations, 1/6-Scale Rigid Tail

For buffet, the Strouhal number is the primary scaling relationship used in determining tunnel conditions.[1] Shown in equation 1, the Strouhal number, *n*, is a nondimensional frequency parameter that is proportional to reduced frequency.

$$n = \frac{f \cdot c}{U} \tag{1}$$

where *f* is frequency in Hz, *c* is characteristic length, and *U* is velocity. A frequency ratio between model and aircraft structural modes and forcing function spectra of unity was chosen, leaving only two variables, *c* and *U*, to be determined. According to the Strouhal number, to match frequency content between aircraft models of different scales, the relationship of *c* divided by *U* must be identical. Since 1/6-scale model was chosen, only one variable, *U*, needed to be determined. According to Reference 1, the dynamic pressure where vertical tail buffeting appeared maximum was roughly 340 psf. Using a value for air density at an altitude of approximately 12,000 feet, velocity was determined. For the case of a 1/6-scale wind-tunnel model that has a frequency ratio of one with the aircraft, the wind speed requirement is 1/6 of the flight speed of the aircraft. For the ACROBAT program, a tunnel speed of 110 feet per second in atmospheric air (14 psf) was used.

General Buffet and Buffeting Characteristics of the 16% F/A-18 Wind-Tunnel Model

Power spectral density plots of the unsteady differential pressures at one station on the tail illustrate the effect of angle of attack on the magnitude of buffet. The buffet at 20 degrees AOA, shown in Figure 7(a), appears broad band compared to the buffet at 34 degrees AOA, shown in Figure 7(b). At 34 degrees AOA, the magnitude of the aerodynamic input (in the lower frequencies) has grown while its peak has shifted to a lower frequency value. These trends of the pressures with angle of attack are consistent with other experimental data.[1, 6]

The pressures, shown in Figure 7 (a)-(b), created the buffeting, or structural response to the buffet, shown in Figure 8 (a)-(b), respectively. At 34 degrees angle of attack, the buffeting shown in Figure 8(b) around 15 Hz, which corresponds to the first bending mode of the vertical tail, has

intensified by 1.5 orders of magnitude above the level at 20 degrees AOA, shown in Figure 8(a). Since the buffet, or force input to the tail, has shifted to a lower frequency with increased angle of attack, as indicated by Figure 7, the resulting vertical tail buffeting mainly consists of a response in the first bending mode, as indicated by comparing Figures 8 (a) and 8 (b). The response in the mode around 58 Hz has not grown significantly with the increase in angle of attack because the magnitude of the pressures in that portion of the spectrum has not increased with increased angle of attack, as seen in Figure 7. These trends agree well with similar results of other wind-tunnel tests. [1, 6]

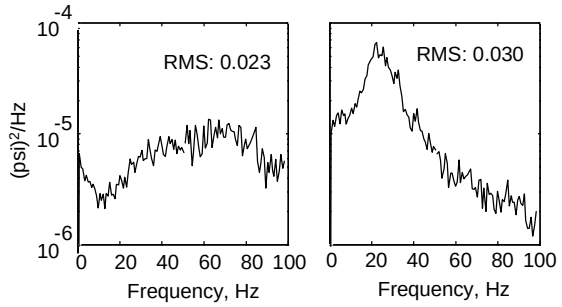

(a) 20 Deg AOA (b) 34 Deg AOA

Figure 7. Differential Pressures Near Mid-Chord, Mid-Span, 1/6-Scale Flexible Tail

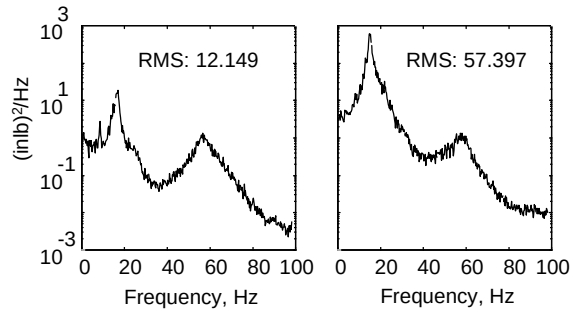

(a) 20 Deg AOA (b) 34 Deg AOA

Figure 8. Root Bending Moment Near Mid-Chord Root, 1/6-Scale Flexible Tail

Chord-Wise Variation in Magnitude of The Unsteady Differential Pressures

The magnitude of the unsteady differential pressure varies with chord location, as seen in Figure 9 for the rigid tail at 34 degrees angle of attack. The peak value and the rms value of the differential pressures near the leading edge are highest, as seen in Figure 9c. As chord location is

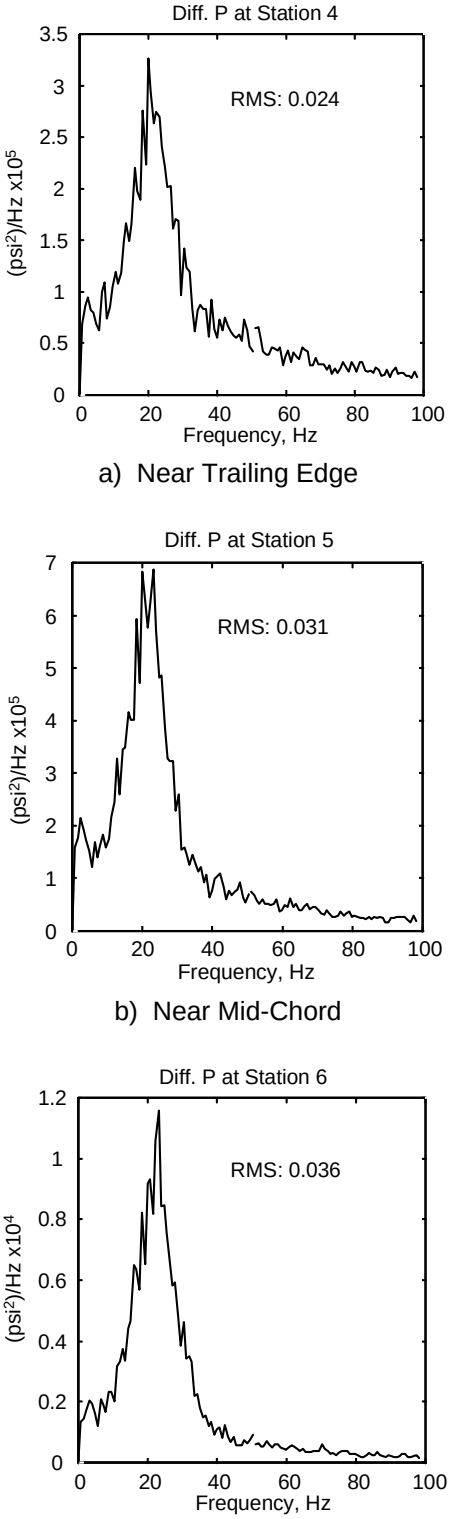

a) Near Trailing Edge

b) Near Mid-Chord

c) Near Leading Edge

Figure 9. Differential Pressures at Three Stations on the Rigid Tail Along The 75% Span Line, 34 Degrees AOA

increased, the peak value and the rms value of the unsteady differential pressure drop, as seen in Figure 9, with the lowest values occurring near the trailing edge. The shape of the power spectral density curves is similar regardless of chord location. Similar results were observed for the flexible tail.

Cross-Correlation Functions For The Rigid Tail

Cross-correlation functions were computed for the differential pressures acquired at the surface stations of the rigid tail, shown in Figure 6. In Figures 10a, the time delays and coefficients are shown for the pressures between stations near the tip. The wave form changes more between stations 1 and 2 than between stations 2 and 3, as indicated by the maximum value of the coefficient (0.651 versus 0.777). Since the time delay between stations 1 and 2 is longer than the time delay between stations 2 and 3 (-0.0031 seconds versus -0.0023 seconds, shown in Figure 10a), the transport velocity between stations 1 and 2 is slower than the transport velocity between stations 2 and 3.

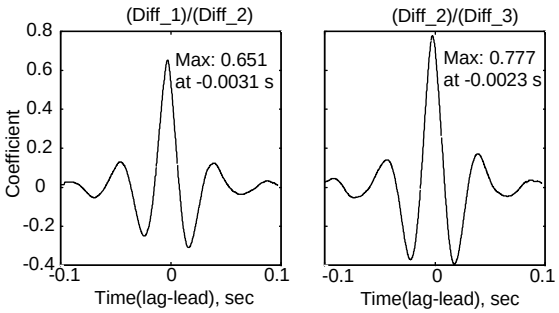

a) Near Tip

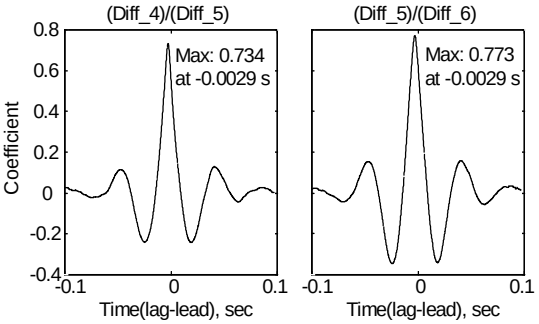

b) Near 75% Span

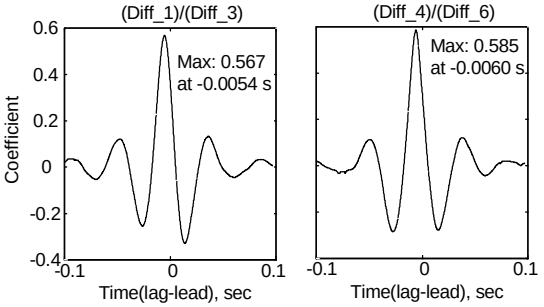

c) Near Trailing Edge with respect to Near Leading Edge, Near Tip and 75% Span

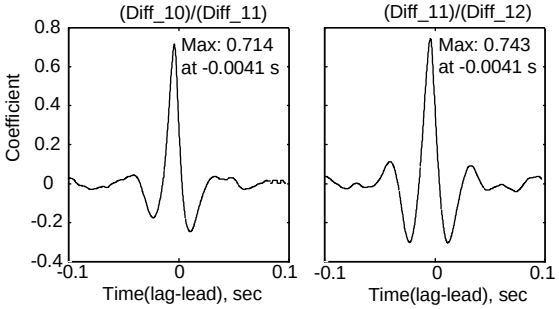

d) Near 40% Span

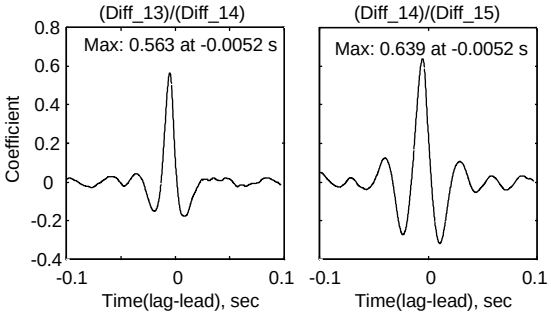

e) Near 25% Span

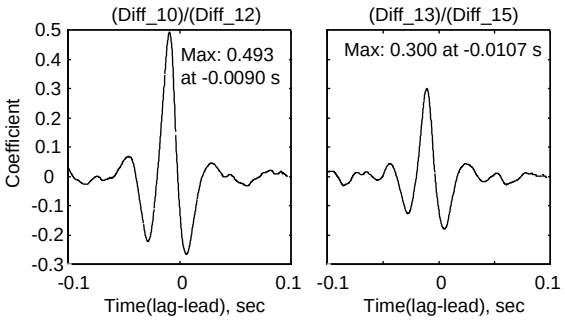

f) Near Trailing Edge with respect to Leading Edge, 40% Span and 25% Span

Figure 10. Cross-Correlation Functions Between Differential Pressures at Stations on Rigid Tail, 34 Deg AOA (See Figure 6 for Station Locations)

Similar results are observed for the pressures at 75% span, as shown in Figure 10b. However, the transport velocities appear identical. In Figure 10c, the cross-correlation functions between trailing edge and leading edge stations are provided for the two span locations just discussed. As a check, the maximum coefficients and their time delays of the two plots in Figure 10c should match the product and the summation of the individual coefficients and time delays, respectively, of Figures 10a and 10b.

The cross-correlation functions for the pressures at lower stations on the tail are provided in Figures 10d through 10f. Since the stations at the lower span are more highly separated than the stations at the higher span, the time delays are longer. There is no noticeable difference in the transport velocities between the stations at 40% span or 25% span, as indicated by the time delays of Figures 10d and 10e. In Figure 10f, the cross-correlation functions between trailing edge and leading edge stations are provided for the two span locations just discussed. As a check, the maximum coefficients and their time delays of the two plots in Figure 10f should match the product and the summation of the individual coefficients and time delays, respectively, of Figures 10d and 10e.

Cross-Spectral Density Functions For The Rigid Tail

The cross-spectral densities between the pressures near the trailing edge with respect to the pressures near the leading edge are provided in Figure 11 for various span locations on the rigid tail shown in Figure 6. The cross-spectral density functions provide similar information as the cross-correlation functions but in the frequency domain. The magnitude illustrates the frequency components of the spectra that dominate the pressure signal, and the phase indicates the number of degrees that a particular frequency component has turned upon reaching the downstream station after passing the upstream station. For instance, the magnitude of (Diff_1)/Diff_3) indicates that the dominant frequency component is around 23 Hz and turns approximately 48 degrees between stations 1 and 3; or, at any time, the 23-Hz component at station 1 lags the 23-Hz component at station 3 by 48 degrees.

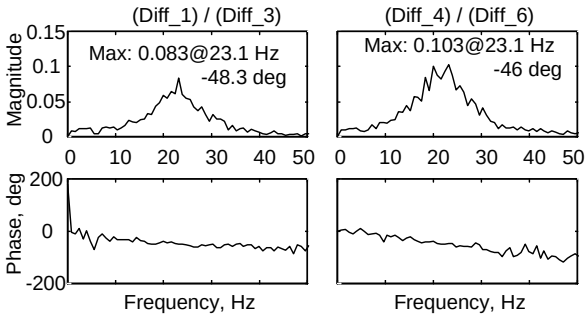

a) Near Trailing Edge with respect to Near Leading Edge, Near Tip and 75% Span

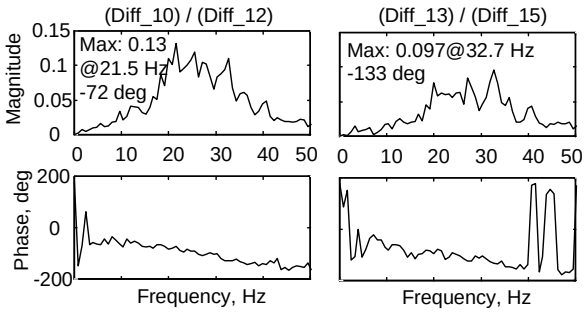

b) Near Trailing Edge with respect to Near Leading Edge, 40% Span and 25% Span

Figure 11. Cross-Spectral Density Functions Between Differential Pressures at Stations on Rigid Tail, 34 Deg AOA (See Figure 6 for Station Locations)

Cross-Correlation and Cross-Spectral Density Functions For The Flexible Tail

Cross-correlation and cross-spectral density functions are shown for the flexible tail to illustrate that flexibility does not appear to affect time and phase delays. For instance, for the rigid tail (shown in Figure 6), the coefficient and time delay for (Diff_5)/(Diff_6) are 0.773 and 0.0029, respectively, as shown in Figure 10b.

Corresponding to these stations on the flexible tail (shown in Figure 5), the coefficient and time delay for (Diff_6)/(Diff_7) are 0.772 and 0.0026, respectively, as shown in Figure 12a. Similar comparisons can be made among other cross-correlation and cross-spectral density functions found in Figures 10 through 13 for corresponding stations on the rigid and flexible tails shown in Figures 5 and 6.

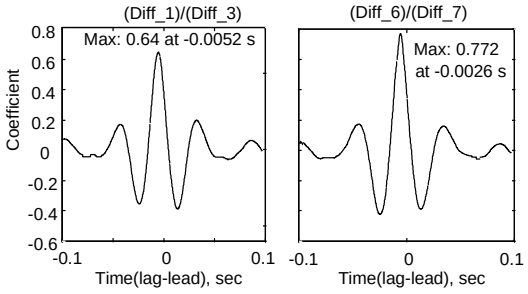

a) Near Tip and 75% Span

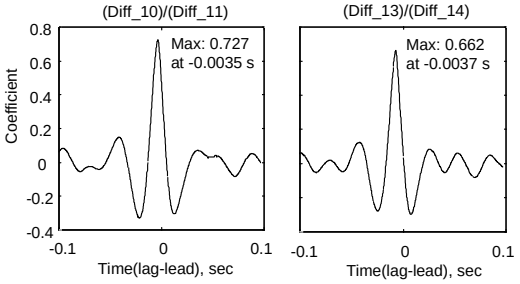

b) Near 60% and 40% Span

Figure 12. Cross-Correlation Functions Between Differential Pressures at Stations on Flexible Tail, 34 Deg AOA (See Figure 5 for Station Locations)

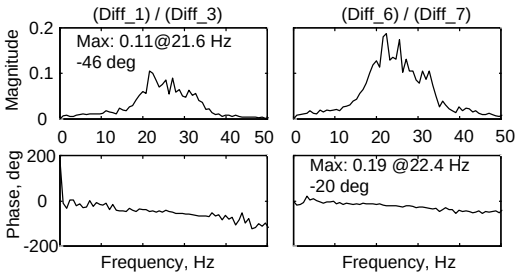

a) Near Tip and 75% Span

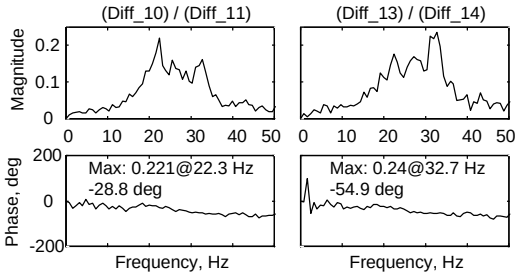

b) Near 60% and 40% Span

Figure 13. Cross-Spectral Density Functions Between Differential Pressures at Stations on Flexible Tail, 34 Deg AOA (See Figure 5 for Station Locations)

Comparing Time Delays With Phase Delays

The time delays can be verified using the distance between the two stations and the transport velocity, as shown in Figure 14.

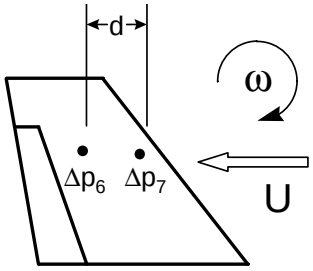

Figure 14. Visualization of Flow, Frequency, and Distance Between Stations

The transport velocity is expected to be less than the freestream velocity of 110 fps because the burst decelerates the flow local to the vertical tail. For the rigid tail at 34 degrees angle of attack, the time delay, in Figure 10c, and phase delay at 23.1 Hz, in Figure 11a for (Diff_4)/(Diff_6), are 0.0060 seconds and 46 degrees, respectively. Stations 4 and 6 are 6.1 inches apart. Using the separation distance and freestream velocity, the time delay is computed using equation 2 as 0.0046 seconds. However, the freestream velocity is considerably faster than the transport velocity, which may be computed as 85 fps using the 6.1-inches separation divided by the 0.0060-seconds time delay. Using the time delay of 0.0060 seconds, the phase delay (at 23.1 Hz) is computed using equation 3. The computed value of 49.8 degrees is close to the 46 degrees picked off the phase plot for the cross-spectral density function shown in Figure 11a.

$$t = d / U \quad (2)$$
$$= 6.1\text{”} / 12\text{ipf}) / 110\text{ fps}$$
$$= 0.0046 \text{ seconds}$$

$$f = w\, t \quad (3)$$
$$= (2\,\pi\, f)\,(d / U)\, 180 / \pi$$
$$= 49.8 \text{ degrees}$$

Comparing Phase Delay Results Of Different Models and Tunnel Conditions

To verify the phase relationships of the partially correlated unsteady differential pressures, comparisons were made with data from other

tests. The time delays and phase delays computed for other wind-tunnel models were compared to some of the results presented above in the cross-correlation and cross-spectral density functions. Using equation 2 above, the ratio of the time delays for the two models may be written as follows:

$$\left(\frac{t_{1/6}}{t_{0.06}}\right) = \frac{d_{1/6}\, U_{0.06}}{d_{0.06}\, U_{1/6}} \qquad (4)$$

Using $d_{1/6}$= 2.66 $d_{0.06}$, and the $U_{0.06}$ = 6 $U_{1/6}$ (Mach 0.6 / Mach 0.1), the time ratio is 16. As noted previously in Figure 2, the time delay between the pressures near the leading edge and the trailing edge on the inboard surface of the 6% rigid tail of Reference 2 is approximately 0.0006 seconds. The time delay for the 1/6-scale rigid tail, shown in Figure 10f for (Diff_10)/(Diff_12) is approximately 0.009 seconds. These two time delays yield a ratio of 15 which is close to the ratio of 16 computed above.

Comparisons between the full-scale wind-tunnel data of Reference 6 and the 1/6-scale phase delays further illustrate the scaling relationship.[10] Using equation 3, the scaling relationship between the phase of the 1/6-scale and the phase of the full-scale cross-spectra is derived, as shown in equation 5. Using $f_{1/6} = f_F$, $d_{1/6}$= 6 d_F, and U_F = 1.5 $U_{1/6}$ (Mach 0.15 / Mach 0.10), the phase ratio is 0.25.

$$\frac{\phi_{1/6-\text{Scale}}}{\phi_{\text{Full}-\text{Scale}}} = \frac{f_{1/6} d_{1/6} U_F}{f_F d_F U_{1/6}} \qquad (5)$$

Shown in Figure 15, the phase at 45 Hz in the cross-spectral density function for the 1/6-scale tail is approximately negative 100 degrees at 20 degrees angle of attack. As shown in Figure 3a, the phase at 45 Hz in the cross-spectral density function for the full-scale tail at 20 degrees angle of attack is approximately negative 400 degrees. The ratio of these two phase values is 0.25. Similarly, for the 1/6-scale model at 34 degrees angle of attack, the phase at 20 Hz in the cross-spectral density function shown in Figure 13a is approximately negative 45 degrees. As shown in Figure 3b, the phase at 20 Hz in the cross-spectral density function for the full-scale tail is approximately negative 180 degrees, which yields a ratio of 0.25.

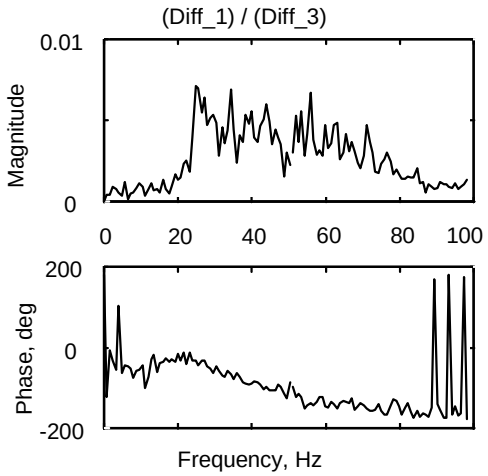

Figure 15. Cross-Spectral Density Functions Between Differential Pressures Near Trailing Edge and Leading Edge, Near Tip, 1/6-Scale Flexible Tail, 20 Degrees Angle of Attack

Conclusions

The unsteady differential pressures measured at high angles of attack on rigid and flexible tails of a 16% F/A-18 wind-tunnel model are not in phase. Cross-correlation and cross-spectral density functions were presented which illustrate the time lags (in the time domain) and phase lags (in the frequency domain) associated with the unsteady differential pressures at stations on vertical tails. The time lags and phase lags are characteristic of a wave and were shown to be functions of the distance between stations and the transport velocity. At a given angle of attack, the partial correlation scales with flight speed, as demonstrated through comparisons of time and phase lags from other wind-tunnel tests at different conditions. For the 16% (1/6-scale) F/A-18 model, tail flexibility does not appear to affect the time delays or the phase delays of the unsteady differential pressures since flexible-tail and rigid-tail results appeared similar. Comparisons with flight data are necessary for substantiating the partial correlation presented herein and for examining further the influence of tail flexibility on pressure correlation.

Acknowledgments

The authors wish to extend their gratitude to the NASA Langley Research Center, especially the

engineers and technicians at the Transonic Dynamics Tunnel, for the support of the 16% F/A-18 wind-tunnel tests mentioned herein. A special personal thanks is extended to Mr. Michael Banford of Wright Laboratory, Wright-Patterson Air Force Base for his staffing and maintaining the pressure data acquisition system used to record the pressures on the vertical tails. Special thanks are extended to Ms. Sheri Hoadley and Ms. Carol Wieseman at NASA Langley Research Center for their analysis software that was used in computing and plotting the 16% F/A-18 pressure results shown herein.

References

1 Zimmerman, N. H., and Ferman, M. A., "Prediction of Tail Buffet Loads for Design Application," Vols. I and II, Rept. No. NADC-88043-60, July 1987.

2 Lee, B. H. K., Brown, D., Zgela, M., and Poirel, D., "Wind Tunnel Investigation and Flight Tests of Tail Buffet on the CF-18 Aircraft", in Aircraft Dynamic Loads Due to Flow Separation, AGARD-CP-483, NATO Advisory Group for Aerospace Research and Development, Sorrento, Italy, April 1990.

3 Ashley, H., Rock, S. M., Digumarthi, R., Chaney, K., and Eggers, A. J. Jr., "Active Control For Fin Buffet Alleviation," WL-TR-93-3099, January 1994.

4 James, K. D. and Meyn, L. A., "Dependence on Integrated Vertical-Tail Buffet Loads For F/A-18 on Sensor Density," SAE Technical Paper 94110, Aerospace Atlantic Conference and Exposition, Dayton, Ohio, April 18-22, 1994.

5 Bean, D. E. and Lee, B. H. K., "Correlation of Wind Tunnel and Flight Test Data For F/A-18 Vertical Tail Buffet," AIAA-94-1800-CP, 12th AIAA Applied Aerodynamics Conference, Colorado Springs, CO, June 20-22, 1994.

6 Pettit, C. L., Banford, M., Brown, D., and Pendleton, E., "Pressure Measurements on an F/A-18 Twin Vertical Tail in Buffeting Flow," Vols 1-4, United States Air Force, Wright Lab., TM-94-3039, Wright Patterson AFB, OH, August 1994.

7 Meyn, L. A. and James, K. D., "Full-Scale Wind-Tunnel Studies of F/A-18 Tail Buffet," Journal of Aircraft, Vol. 33, No. 3, May-June 1996.

8 Moses, R. W., "Active Vertical Tail Buffeting Alleviation on a Twin-Tail Fighter Configuration In a Wind Tunnel," presented at the CEAS International Forum on Aeroelasticity and Structural Dynamics 1997, 17-20 June 1997, Rome, Italy.

9 Bendat, J. S. and Piersol, A. G., Engineering Applications of Correlation and Spectral Analysis, Second Edition, John Wiley & Sons, Inc., 1993.

10 Moses, R. W. and Pendleton, E., "A Comparison of Pressure Measurements Between a Full-Scale and a 1/6-Scale F/A-18 Twin Tail During Buffet," presented at the 83rd Meeting of the Structures And Materials Panel (SMP) of the Advisory Group for Aerospace Research and Development (AGARD), Florence, Italy, September 2-6, 1996.